Accurate modeling of benchmark x-ray spectra from highly charged ions of tungsten

Yuri Ralchenko,* Joseph N. Tan, J. D. Gillaspy, and Joshua M. Pomeroy
Atomic Physics Division, National Institute of Standards and Technology, Gaithersburg, Maryland 20899-8422, USA

Eric Silver
Harvard-Smithsonian Center for Astrophysics, 60 Garden Street, Cambridge, Massachusetts 02138, USA
(Received 31 August 2006; published 26 October 2006)

We present detailed collisional-radiative modeling for a benchmark x-ray spectrum of highly charged tungsten ions in the range between 3 and 10 Å produced in an electron beam ion trap (EBIT) with a beam energy of 4.08 keV. Remarkably good agreement between calculated and measured spectra was obtained without adjustable parameters, highlighting the well-controlled experimental conditions and the sophistication of the kinetic simulation of the non-Maxwellian tungsten plasma. This agreement permitted the identification of spectral lines from Cu-like W^{45+} and Ni-like W^{46+} ions, led to the reinterpretation of a previously known line in Ni-like ion as an overlap of electric-quadrupole and magnetic-octupole lines, and revealed subtle features in the x-ray spectrum arising from the dominance of forbidden transitions between excited states. The importance of level population mechanisms specific to the EBIT plasma is discussed as well.

DOI: 10.1103/PhysRevA.74.042514 PACS number(s): 32.30.Rj, 39.10.+j, 52.59.−f

Highly charged ions of heavy elements represent an important field of atomic physics that offers numerous challenges from both theoretical and practical viewpoints [1]. Their basic atomic characteristics, such as energies and radiative transition probabilities, are strongly influenced by relativistic and even quantum-electrodynamic (QED) effects, which often bring about new spectral patterns that are very different from the spectra of light elements. For instance, the forbidden radiative transitions in such systems are enhanced by many orders of magnitude relative to electric-dipole allowed transitions, while the coupling of angular momenta is frequently dominated by the spin-orbit rather than the Coulomb interaction. Also, high-resolution x-ray spectra of highly charged ions are now readily observed in the solar corona and other astrophysical sources, serving as important diagnostic tools for determining elemental composition and plasma characteristics.

Of particular interest are some heavy elements (e.g., tungsten) selected as candidates for components of the next generation fusion reactor, ITER, especially in the divertor region [2]. The erosion of the reactor elements results in contamination of the confined plasma, which heats the plasma-facing components during operation. As the radiative emission rate strongly increases with the ion charge ($A_{rad} \sim Z^4$), detailed information about the emission processes due to heavy impurities is crucial for the evaluation of radiative losses, knowledge of which is imperative for achievement of sustained energy production.

Precise spectra of highly charged ions measured under well-diagnosed conditions represent extremely valuable benchmarks for validation and verification of complex computer codes for plasma kinetic simulations and spectroscopic diagnostics of hot plasmas. Since the overwhelming majority of laboratory and astrophysical plasmas are subject to various instabilities and gradient effects that very often obscure the experimental picture, the kinetic code comparisons are mostly limited to ideal "computational experiments" [3] that, so far, have showed significant differences between various models, especially for heavy elements. To this end, accurately measured spectra from highly charged ions may direct the future development of plasma population kinetic codes used in magnetic and inertial confinement fusion, astrophysics, lithography, and other applications. In this paper, we present the essential features in detailed modeling of a broadband, high-resolution measurement of x-ray emission lines from tungsten ions produced by electron impact in the electron beam ion trap (EBIT) operating at the National Institute of Standards and Technology (NIST).

Results under well-characterized conditions are presented for the case in which the electron beam in the EBIT is accelerated to 4.08 keV, near the ionization threshold of Ni-like W^{46+}. A quantum calorimeter (or microcalorimeter) is used to detect x-ray photons emitted by the highly charged ions of tungsten, measuring the spectrum from 3 to 10 Å, as described below. The earliest x-ray spectra of highly charged W ions were observed in exploding wires [4] and laser-produced plasmas [5,6]. Recently, spectra from a few ionization stages were obtained on the ASDEX tokamak in the spectral range from 7 to 10 Å [7], and on an EBIT at the Lawrence Livermore National Laboratory (LLNL), allowing the identification of features in the spectral range from 5 to 6 Å [8]. An independent effort at LLNL is also studying the spectrum between 3.5 and 8 Å obtained from W ions excited in an EBIT with a beam energy of 3.9 keV [9]. Also, a large compilation of spectroscopic data from ions W II to W LXXIV is currently under preparation [10].

Accurate measurements of relatively simple x-ray spectra are obtainable using an EBIT, which essentially confines highly charged ions in the electromagnetic fields of a Penning trap modified by a coaxial electron beam which has a density high enough to dominate the radial confinement of the ions. In the present work, highly charged ions are produced, trapped, and excited by the electron beam (94 mA), which is accelerated to an energy of about 4.0 keV in the

*Electronic address: yuri.ralchenko@nist.gov

central trap region. Charge stage production and level excitation can be made with good selectivity because the electron beam is nearly mono-energetic, with a tunable energy distribution which can be as narrow as 35 eV under some conditions. The electron current density is intensified by a magnetic field of 2.7 T, generated by a pair of coaxial Helmholtz coils. Viewports with spectroscopic windows are in the midplane of the trap. Liquid helium is used to make the Helmholtz coils superconducting, cool the trap electrodes, and maintain a high vacuum environment. Tungsten is loaded into the NIST EBIT using a two-wire metal vapor vacuum arc (MeVVA) [11] with eight independent cathodes, each selectable without downtime. Initially, singly charged W ions are extracted in bunches from the MeVVA ion source, and accelerated into the trapping region. Ions are confined along the axis by a potential well 280 V deep. At the beginning of each loading cycle, as an ion bunch is extracted from the MeVVA, the axial potential well is opened momentarily by pulsing one of the electrodes to form a decelerating potential ramp for capturing the ion bunch. Subsequently, the captured W ions are further ionized, stepwise to increasingly higher charge states until the electron beam energy is below the threshold of the next ionization stage. To minimize breeding of contaminant ions, the ion trap is emptied every 3173 ms by keeping the axial well opened for 10 ms prior to the start of the next loading cycle.

To measure the spectrum, x-ray photons emitted in the energy range from 0.2 to 10 keV are counted with high-energy resolution and near-unity quantum efficiency using a microcalorimeter. We use a neutron transmutation-doped (NTD) germanium microcalorimeter with a linear 1×4 array of Sn absorbers, located about 74 cm from the trapped ions [11,12]. Figure 1(a) shows the observed spectrum in the spectral range of 3–10 Å. One advantage of using a microcalorimeter is its insensitivity to the polarization of the x-ray emission associated with the well-defined quantization axis along the electron beam which excites the trapped ions. The development and operation of nondispersive x-ray spectrometers are discussed elsewhere [12–14]. In brief, x-ray photons are absorbed in 0.35 mm$\times$0.35 mm$\times7$ μm size foils of superconducting tin and converted into heat. The temperature rise due to each absorbed photon is measured with an NTD-Ge thermistor which is attached to the underside of the absorber. This NTD-Ge microcalorimeter has a quantum efficiency of 95% at 6 keV, and attained an energy resolution of $\sim$5 eV when stabilized at 60 mK to within 5 μK during data acquisition [11]. A two-stage adiabatic demagnetization refrigerator (ADR) is used to stabilize the temperature near 60 mK for over 170 000 s before the ADR must be recycled.

A reliable modeling of the x-ray emission from the highly charged ions in EBIT can only be achieved through synthesis of advanced collisional-radiative modeling and accurate atomic calculations. The unique properties of the EBIT plasma, and most of all, the narrow non-Maxwellian electron energy distribution function (EEDF) with a low electron density ($N_e\sim10^{11}$ cm^{-3}), allow one to drastically modify the relative importance of various atomic processes compared to what is typical for hot thermal plasmas. For instance, dielectronic recombination that is the primary recombination channel in high-temperature Maxwellian plasmas is completely

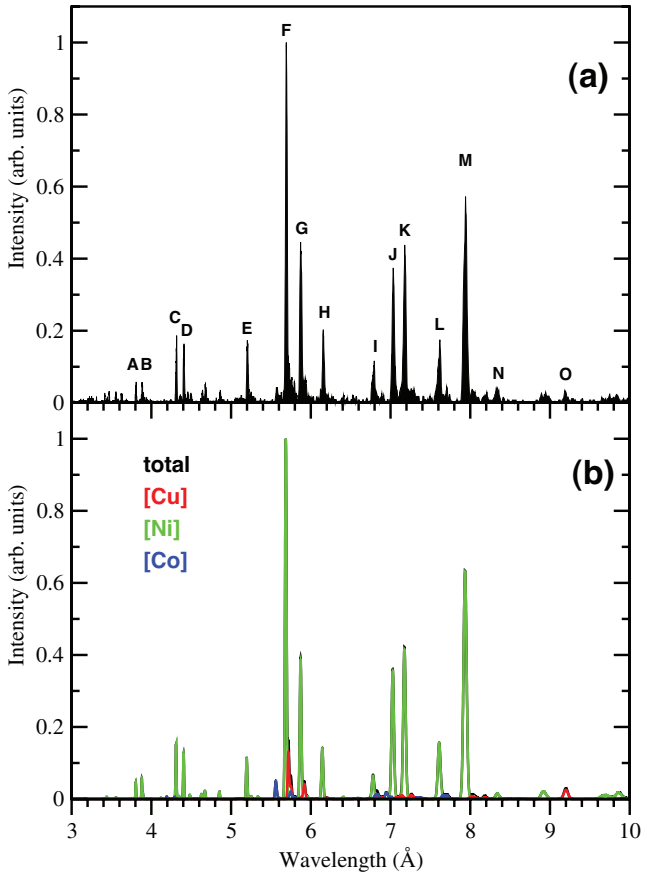

FIG. 1. (Color online) (a) Measured spectrum at beam energy 4.08 keV; and (b) calculated spectrum at beam energy 4.06 keV. Contributions from Cu-, Ni-, and Co-like ions of W are shown in different colors.

negligible in the present experimental environment because it requires electrons with a specific, resonant energy outside the range of the selected energy-localized EEDF. Further, as will be shown below, electron-impact excitation from the inner shells that is almost never important in thermal plasmas may strongly affect the observed spectrum. On the other hand, as typical in low-density coronal plasmas, both three-body recombination and electron-impact deexcitation are completely negligible compared to radiative recombination and spontaneous radiative decays, respectively.

It is well-known that in thermal plasmas the typical maximal abundance temperature for an ion with ionization energy I_Z is of the order of $I_Z/10$ only (see, e.g., [15]), and therefore the amount of electrons with relatively high energies ($\sim I_Z$) is very small. Besides, the ionization distribution in Maxwellian plasmas normally has a bell-like shape so that a number of ions with charges larger or smaller than that of the most abundant state are significantly populated. In the EBIT plasma, however, due to its almost monoenergetic EEDF, the ions in a specific charge stage Z are only produced when the beam energy exceeds the ionization potential of the previous ion, $E_{beam}>I_{Z-1}$, so that the ionization distribution is sharply cut. (Electron-impact ionization from the excited states can be ignored for highly charged ions in dilute plasmas.) In addition, practically all plasma electrons in EBIT are highly

energetic with $E \sim I_Z$, and this results in a very different distribution of level populations compared to thermal Maxwellian plasmas.

The ionization distribution, level populations, and line intensities in the EBIT plasma of tungsten are calculated here with a collisional-radiative code NOMAD [16] that allows kinetics simulations for an arbitrary EEDF. In general, NOMAD solves a time-dependent system of differential rate equations for atomic states taking into account various plasma effects, e.g., source geometry, opacity effects, and ionization potential lowering. Here, due to a very low particle density, most of the plasma effects can be safely neglected. Since the EBIT plasma in the present experiment reaches an equilibrium state within fractions of a second (cf. the plasma lifetime of about 3 s), NOMAD simulations were performed for steady state conditions. The beam EEDF was approximated by a Gaussian function with a full width at half-maximum of 60 eV. The NOMAD code is capable of using various sources of atomic data for calculation of rate matrix elements. Since no existing database can provide the required extensive set of energy levels, transition probabilities, and collisional cross sections for the relevant ions of W, the input data for collisional-radiative simulations need to be generated using accurate atomic codes. Here we make use of the flexible atomic code (FAC) to calculate all atomic characteristics for about 2500 energy levels and hundreds of thousands of transitions in ions from Zn-like W^{44+} to Mn-like W^{49+}. The theoretical techniques and approximations implemented in FAC are discussed in detail in Ref. [17] and references therein. Most importantly, the key methods used in FAC, such as, e.g., the modified relativistic Dirac-Fock-Slater method for calculation of atomic wave functions with account of the QED effects, are well-suited to highly charged ions of heavy elements. Another essential feature that significantly enhances reliability of the modeling is that FAC produces a complete and consistent set of all structure and collisional parameters required for solving the NOMAD rate equations. As mentioned above, the importance of radiative forbidden transitions greatly increases with the ion charge. Therefore, for a comprehensive simulation of all possible spectral features, in addition to the allowed electric-dipole ($E1$) transitions, our simulations include the electric-quadrupole ($E2$), magnetic-dipole ($M1$), magnetic-quadrupole ($M2$), and magnetic-octupole ($M3$) transitions as well.

Figure 1(b) presents the calculated spectrum at theoretical beam energy of 4.06 keV as a sum of contributions from the most populated ion stages—namely, Cu-like [Cu], Ni-like [Ni], and Co-like [Co] ions of W—all of which are also superimposed distinctly. Comparison shows that the strongest lines in the observed spectrum, Fig. 1(a), are emitted by the Ni-like W^{46+} that constitutes about 78% of the total ion population. This is due to the fact that the electron beam produces and excites Ni-like W ions efficiently at an energy of about 4 keV, which is well above the ionization potential of Cu-like W ions ($I_{Cu} \approx 2.414$ keV), and near the ionization threshold of Ni-like W ions ($I_{Ni} \approx 4.057$ keV). Our simulations show that the relative intensities of the [Ni] lines are insensitive to small variations near this beam energy as the excitation cross sections from the ground and metastable

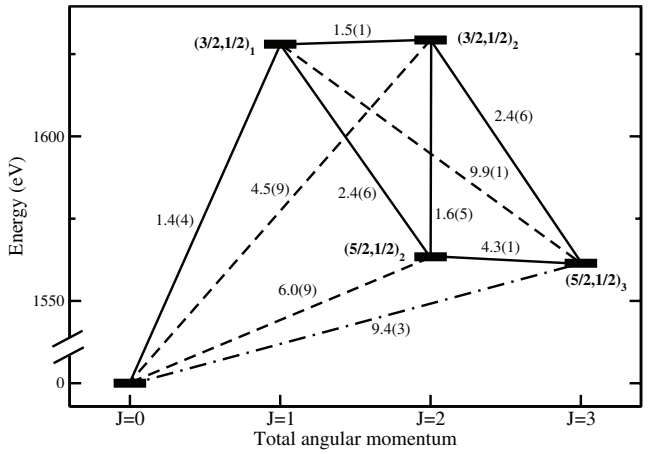

FIG. 2. Energy diagram for the $3d^{10}$ (ground state configuration) and $3d^9 4s$ (first excited configuration) levels in W^{46+}. Solid lines: $M1$ transitions; dashed lines: $E2$ transitions; and dot-dashed line: $M3$ transition. Transition probabilities (in s^{-1}) are given next to the corresponding lines. Notation $a(b)$ means $a \times 10^b$.

states change very little over several tens of eV. As typical for coronal plasmas, such excitations that may be followed by radiative cascades are the primary channel for population of atomic levels. On the other hand, the intensities of the [Co] lines relative to the [Ni] lines strongly depend both on the amount of electrons with energies above the ionization threshold of W^{46+} and on their energy since the ionization cross section rapidly changes in the near-threshold region. Hence the intensity ratio between the strongest $3d^9$-$3d^8 4f$ [Co] line at 5.575 Å and [Ni] lines was used to determine the theoretical mean beam energy of 4.06 keV, which is well within the 2% uncertainty of the accelerating voltage applied to the drift tubes. In the absence of any ions there could be an additional systematic shift in the actual beam energy of up to −240 eV due to the space charge of the dense electron beam; however, the good agreement between the prediction and the nominal beam energy suggests, as expected, that the space charge is nearly completely neutralized by the positive ions confined in the beam. Under these conditions, the Cu- and Co-like ions constitute about 15% and 6% of the total population, respectively. Comparing Fig. 1(a) and 1(b), we find remarkably good agreement between the calculated and measured spectra, both for wavelengths and relative line intensities. Note that this is attained with no adjustable parameters other than the beam energy. This results in part from the well-characterized experimental conditions, and in part from the advanced collisional-radiative modeling capable of representing all of the relevant processes adequately.

The strongest 15 emission lines in Fig. 1(a) are labeled by letters and listed in Table I. Most of the lines in Fig. 1(a) are due to the transitions into the ground states of corresponding ions and were previously identified [5–7,18–20]. The detailed spectrum analysis allowed us to identify two new lines (L and N) and reidentify another line (M). The line identifications given in jj-coupling are based on the good agreement between calculated and observed wavelengths, and on a very good match of relative line intensities. A well-resolved spectral line N at 8.337 Å agrees with the calculated wavelength

TABLE I. The strongest lines in the experimental spectrum of Fig. 1. Lines $A-N$ are from the Ni-like W^{46+}, line O from the Cu-like W^{45+}. Experimental wavelength uncertainties in units of the last digit are given in parenthesis.

	Wavelength (Å)					
Line	Present expt.	Present theory	Other expt.	Theory[g]	Theory[h]	Transition
A	3.800(2)	3.805	3.803(2)[a]			$3d^{10}\,{}^1S_0$-$3d^9 6f(3/2,5/2)_1$
B	3.878(2)	3.880	3.877(2)[a]			$3d^{10}\,{}^1S_0$-$3d^9 6f(5/2,7/2)_1$
C	4.309(2)	4.309	4.309(2)[a]		4.3083	$3d^{10}\,{}^1S_0$-$3d^9 5f(3/2,5/2)_1$
D	4.403(2)	4.405	4.406(2)[a]		4.4043	$3d^{10}\,{}^1S_0$-$3d^9 5f(5/2,7/2)_1$
E	5.203(3)	5.196	5.203(2)[a]	5.201	5.1944	$3p^6 3d^{10}\,{}^1S_0$-$3p^5 3d^{10} 4d(3/2,5/2)_1$
F	5.691(2)	5.686	5.6913(8)[b]	5.689	5.6833	$3d^{10}\,{}^1S_0$-$3d^9 4f(3/2,5/2)_1$
G	5.872(2)	5.872	5.8715(8)[b]	5.870	5.8717	$3d^{10}\,{}^1S_0$-$3d^9 4f(5/2,7/2)_1$
H	6.155(4)	6.145	6.154(5)[c]	6.154	6.1465	$3d^{10}\,{}^1S_0$-$3p^5 3d^{10} 4s(3/2,1/2)_1$
I	6.785(5)	6.780	6.779(3)[d]	6.778	6.7806	$3d^{10}\,{}^1S_0$-$3d^9 4p(3/2,3/2)_1$
J	7.030(4)	7.028	7.028(3)[d]	7.027	7.0296	$3d^{10}\,{}^1S_0$-$3d^9 4p(5/2,3/2)_1$
K	7.174(4)	7.175	7.1733(3)[e]	7.174	7.1760	$3d^{10}\,{}^1S_0$-$3d^9 4p(3/2,1/2)_1$
L	7.607(6)	7.610		7.610	7.6135	$3d^{10}\,{}^1S_0$-$3d^9 4s(3/2,1/2)_2$
M	7.930(5)	7.930^{E2}, 7.940^{M3}	7.93(2)[f]	7.929^{E2}, 7.938^{M3}	7.9354^{E2}	$3d^{10}\,{}^1S_0$-$3d^9 4s(5/2,1/2)_2$, $3d^9 4s(5/2,1/2)_3$
N	8.326(11)	8.333				$3d^9 4p(3/2,1/2)_1$-$3d^9 6d(3/2,3/2)_0$
O	9.174(16)	9.200	9.18(2)[f]		9.1949	$3d^{10} 4p\,{}^2P_{3/2}$-$3d^9 4s^2\,{}^2D_{5/2}$

[a]Reference [18].
[b]Reference [19].
[c]Reference [5].
[d]Reference [6].
[e]Reference [20].
[f]Reference [7].
[g]Reference [21].
[h]Reference [22].

of $\lambda_{th}=8.333$ Å for the $3d^9 4p(3/2,1/2)_1$-$3d^9 6d(3/2,3/2)_0$ transition in the Ni-like W ion. The presence of four other relatively strong $3d^{10}4p-3d^{10}6d$ transitions with wavelengths between 8.904 and 8.937 Å is also predicted by the simulations. Indeed, the measured spectrum shows a wide, isolated structure centered at $\lambda \approx 8.93$ Å. However, the spectral resolution required to separate these lines is beyond the scope of the present experimental setup. Several weaker lines from the Cu-like and Co-like ions are also clearly resolved, for example, the line O at 9.192 Å which corresponds to the two-electron $3d^{10}4p_{3/2}$-$3d^9_{5/2}4s^2$ transition in Cu-like W. Table I also presents the data from the compilation of W data [10], the latest theoretical results obtained by relativistic many-body perturbation theory [21], and the relativistic model-potential HULLAC code [22]. A comparison shows that, on average, the agreement between our calculated and measured wavelengths is within 0.11%. Note also that the identification of the lines *F* and *H* in Ref. [21] should be reversed, as corrected in Table I.

Electric-dipole-forbidden lines find wide applications in physics [23], in particular, in plasma diagnostics where they often serve as a reliable tool for determination of electron density (see, e.g., [24]). The prominent [Ni] lines of W ions at 7.614 and 7.939 Å originate from the lowest excited configuration $3d^9 4s$. Since the four levels in this configuration have the same parity as the ground state $3d^{10}$, they can only decay via forbidden radiative transitions. The doublet energy structure within the excited configuration is diagrammed in Fig. 2, illustrating the almost pure *jj*-coupling for these levels, as is often found in the isoelectronic sequences of closed shell ions. For this particular system the pair coupling is enhanced even more due to the large charge of the W nucleus. The line *L* at 7.614 Å corresponds to the *E*2 transition $3d^{10}$-$3d^9 4s(3/2,1/2)_2$. The experimental wavelength confirms the theoretical value of $\lambda_{th}=7.610$ Å with a predicted transition probability of 4.5×10^9 s^{-1}. While interconfiguration *E*2 transitions are generally much stronger than the interconfiguration *M*1 transitions, this fact, nonetheless, is not sufficient to explain the absence of the nearby *M*1 transition $3d^{10}$-$3d^9 4s(3/2,1/2)_1$ at $\lambda_{th}=7.616$ Å with a transition probability of $A=1.4\times10^4$s^{-1}. Our calculations indicate a very small branching ratio for this missing line as its upper level $3d^9 4s(3/2,1/2)_1$ is predominantly depopulated by a strong intraconfiguration *M*1 transition to $3d^9 4s(5/2,1/2)_2$ with $A=2.4\times10^6$ s^{-1} (see Fig. 2). Moreover, this $3d^9 4s(5/2,1/2)_2$-$3d^9 4s(3/2,1/2)_1$ transition is crucial for the accurate determination of the *M* line intensity. In addition to being the dominant depopulation mechanism (almost 100%) for the upper $J=1$ state, this decay channel also supplies about 30% of the population influx to the $3d^9 4s(5/2,1/2)_2$ excited state, a much larger contribution than the 0.7% influx due to direct electron-impact excitation from the ground state. Hence turning this process off would drastically change the populations of both excited states and would cause the intensity ratio of the 7.614 and 7.939 Å lines to be a factor of 2 smaller than the observed line ratio.

This is a rare and important example where forbidden radiative transitions between *excited* states are essential for accurate spectral modeling.

The detailed analysis necessitates a reinterpretation of the forbidden line at 7.939 Å—one of the brightest lines in Fig. 1(a)—which was previously identified as an $E2$ transition $3d^{10}$-$3d^{9}4s(5/2,1/2)_2$ [7,10]. The calculated wavelength for this transition, 7.930 Å, is very close to the theoretical magnetic-octupole ($M3$) $3d^{10}$-$3d^{9}4s(5/2,1/2)_3$ line at 7.940 Å. Since the instrumental line broadening is $\Delta\lambda \approx 0.015$ Å, these lines are expected to overlap significantly and be observed as a single line. The collisional-radiative simulations for the present EBIT conditions indicate that the $E2$ and $M3$ lines have comparable intensities with a ratio of approximately $I(E2):I(M3) \approx 4:3$. Therefore neglecting the $M3$ line in the spectrum synthesis would result in a noticeable discrepancy between theory and measurements. As supporting evidence, the width of the measured line is almost a factor of 2 larger than the widths of other neighboring lines, indicating the presence of at least two transitions. Hence the measured line at 7.939 Å should be reidentified as an overlap of the $E2$ and $M3$ lines, as listed in Table I. As a theoretical note, the presently calculated transition probabilities for these lines $A(M3) \approx 9.4 \times 10^3$ s^{-1} and $A(E2) \approx 6.0 \times 10^9$ s^{-1} agree well with the recent many-body perturbation theory values of 8.22×10^3 s^{-1} and 5.32×10^3 s^{-1}, respectively [21].

An excellent agreement between simulated and experimental spectra allows us to unambiguously determine the relative importance of different population mechanisms for specific levels. As expected for direct dipole-allowed excitations, the $3d^{9}nf$ states with the total angular momentum $J=1$ are preferentially (about 99%) excited from the ground state $3d^{10}$ by the electron impact. However, the $3d^{9}4p$ levels that are also connected by dipole-allowed transitions to the ground state receive only about 5% to 9% of the total population influx through ground state excitation. Rather, the majority of the flux into the $3d^{9}4p$ levels is due to the $\Delta n=0$ radiative decays from the $3d^{9}4d$ levels, which in turn are efficiently populated by the strong monopole $3d$-$4d$ excitations from the ground state. Note that it is this population mechanism that is responsible for population inversion in collisional x-ray lasers based on Ni-like ions [25].

A careful examination of population mechanisms in the EBIT plasma can expose some processes that are difficult to detect in thermal plasmas. Consider, for instance, the H line originating from the $3p^{5}3d^{10}4s(3/2,1/2)_1$ state. The direct $3p$-$4s$ excitation from the ground state contributes less than one-third of the total population influx. While radiative decays from the excited $3p^{5}3d^{10}np$ states are important as well, we found that a good agreement with the experimental data could only be achieved when the inner-shell $\Delta n=0$ radiative transitions $3s^{2}3p^{5}3d^{10}4s$-$3s3p^{6}3d^{10}4p$ are taken into account. Analysis shows that the dominant mechanism for populating the $3s3p^{6}3d^{10}4p$ states is the direct $3s$-$4p$ electron-impact excitation from the $3s$ inner shell of the ground state. Again, in a Maxwellian plasma there would be very few energetic electrons above the corresponding excitation threshold, and therefore such deep-inner-shell excitations are normally ignored in modeling. For the EBIT plasma conditions, however, they become critically important in spectrum simulations.

In summary, using a microcalorimeter spectrometer, a high resolution x-ray spectrum in the range between 3 and 10 Å was obtained from highly charged tungsten ions stored in an EBIT at a beam energy 4.08 keV. A detailed accounting of the physical processes in this experiment was carried out using advanced atomic and plasma codes. The remarkably good agreement between calculated and measured spectra without free parameters is made possible by the well-controlled experimental conditions as well as by the availability of computer codes capable of implementing an accurate theoretical representation of all the relevant atomic and plasma processes. The detailed modeling of a well-characterized laboratory source was instrumental in the identification of new lines from Ni- and Cu-like W ions, allowed us to explain a previously known line as an overlap of forbidden $E2$ and $M3$ lines, and revealed subtle features in the x-ray spectrum arising from forbidden transitions between excited states. It demonstrates that the relatively simple broadband spectra from ions stored in an EBIT can serve as a powerful test-bed for benchmarking the development of theoretical models and computer codes to provide accurate representations of more complex systems, such as those needed in modeling open-shell atoms and ions.

This work was supported in part by the Office of Fusion Energy Sciences of the U.S. Department of Energy. We are grateful to J. Reader and U. I. Safronova for valuable discussions and to A. Kramida for providing unpublished compilation data on tungsten spectra.

[1] J. D. Gillaspy, J. Phys. B **34**, R93 (2001).
[2] V. Phillips, Phys. Scr., T, **123**, 24 (2006).
[3] Yu. Ralchenko, R. W. Lee, and C. Bowen, in *14th APS Topical Conference on Atomic Processes in Plasmas*, edited by J. S. Cohen *et al.*, AIP Conf. Proc. No. 730 (AIP, Melville, NY, 2004); C. Bowen, R. W. Lee, and Yu. Ralchenko, J. Quant. Spectrosc. Radiat. Transf. **99**, 102 (2006).
[4] P. G. Burkhalter, C. M. Dozier, and R. D. J. Nagel, Phys. Rev. A **15**, 700 (1977).
[5] A. Zigler, H. Zmora, N. Spector, M. Klapisch, J. L. Schwob, and A. Bar-Shalom, J. Opt. Soc. Am. **70**, 129 (1980).
[6] P. Mandelbaum, M. Klapisch, A. Bar-Shalom, J. L. Schwob, and A. Zigler, Phys. Scr. **27**, 39 (1983).
[7] R. Neu, K. B. Fournier, D. Schlögl, and J. Rice, J. Phys. B **30**, 5057 (1997).
[8] P. Neill, C. Harris, A. S. Safronova, S. Hamasha, S. Hansen, U. I. Safronova, and P. Beiersdorfer, Can. J. Phys. **82**, 931 (2004).

[9] T. Hoppe, A. Safronova, U. I. Safronova, P. Neill, C. Harris, P. Beiersdorfer, G. Brown, K. R. Boyce, R. Kelly, C. Kilbourne, and S. Porter, Bull. Am. Phys. Soc. **50**, 132 (2005).
[10] A. E. Kramida and T. Shirai (unpublished).
[11] G. E. Holland, C. N. Boyer, J. F. Seely, J. N. Tan, J. M. Pomeroy, and J. D. Gillaspy, Rev. Sci. Instrum. **76**, 073304 (2005).
[12] J. N. Tan, E. Silver, J. Pomeroy, J. M. Laming, and J. Gillaspy, Phys. Scr., T **119**, 30 (2005).
[13] E. Silver, G. Austin, J. Beeman, F. Goulding, E. E. Haller, D. Landis, and N. Madden, Nucl. Instrum. Methods Phys. Res. A **545**, 683 (2005).
[14] See, for example, review by D. Twerenbold, Rep. Prog. Phys. **59**, 349 (1996).
[15] I. I. Sobel'man, L. A. Vainshtein, and E. A. Yukov, *Excitation of Atoms and Broadening of Spectral Lines* (Springer-Verlag, Berlin, 1995).
[16] Yu. V. Ralchenko and Y. Maron, J. Quant. Spectrosc. Radiat. Transf. **71**, 609 (2001).
[17] M. F. Gu, in *Proceedings of the 14th APS Topical Conference on Atomic Processes in Plasmas*, edited by J. Cohen, S. Mazevet, and D. Kilkrease, AIP Conf. Proc. No. 730 (AIP, Melville, NY, 2004), p. 127.
[18] N. Tragin, J.-P. Geindre, P. Monier, J.-C. Gauthier, C. Chenais-Popovics, J.-F. Wyart, and C. Bauche-Arnoult, Phys. Scr. **37**, 72 (1988).
[19] R. Butzbach, H. Daido, E. Förster, Y. Gu, G. Huang, Y. Kato, F. Koike, S. Sebban, H. Tang, I. Uschmann, M. Vollbrecht, and S. Wang, *Inst. Phys. Conf. Ser., No. 159, X-ray Lasers Conference, Kyoto, Japan* (IOP, Bristol, 1999), p. 463.
[20] S. R. Elliott, P. Beiersdorfer, B. J. MacGowan, and J. Nilsen, Phys. Rev. A **52**, 2689 (1995).
[21] U. I. Safronova, A. S. Safronova, S. M. Hamasha, and P. Beiersdorfer, At. Data Nucl. Data Tables **92**, 47 (2006).
[22] K. B. Fournier, At. Data Nucl. Data Tables **68**, 1 (1998).
[23] J. Sucher, Rep. Prog. Phys. **41**, 1781 (1978), for example, gives a review of the theory for $M1$ transitions and the important roles they play in atomic and particle physics.
[24] A. Gabriel and C. Jordan, Mon. Not. R. Astron. Soc. **145**, 241 (1969).
[25] R. C. Elton, *X-ray Lasers* (Academic Press, Inc., Boston, 1990).